the FEBS Journal

Sialylation of urinary prothrombin fragment 1 is implicated as a contributory factor in the risk of calcium oxalate kidney stone formation

Dawn Webber[1], Catherine M. Radcliffe[2], Louise Royle[2], Gemma Tobiasen[2], Anthony H. Merry[2], Allen L. Rodgers[1], Edward D. Sturrock[3], Mark R. Wormald[2], David J. Harvey[2], Raymond A. Dwek[2] and Pauline M. Rudd[2]

1 Department of Chemistry, University of Cape Town, South Africa
2 Department of Biochemistry, Glycobiology Institute, University of Oxford, UK
3 Division of Medical Biochemistry and Institute of Infectious Disease and Molecular Medicine, University of Cape Town, South Africa

Keywords
calcium oxalate; glycosylation; kidney stones; sialic acid; urinary prothrombin fragment 1

Correspondence
P. M. Rudd, Glycobiology Institute, Department of Biochemistry, South Parks Road, University of Oxford, Oxford, OX1 3QU, UK
Fax: +44 1865 275796
Tel: +44 1865 275340
E-mail: pauline.rudd@bioch.ox.ac.uk

(Received 2 February 2006, revised 5 April 2006, accepted 10 May 2006)

doi:10.1111/j.1742-4658.2006.05314.x

Urinary glycoproteins are important inhibitors of calcium oxalate crystallization and adhesion of crystals to renal cells, both of which are key mechanisms in kidney stone formation. This has been attributed to glycosylation of the proteins. In South Africa, the black population rarely form stones (incidence < 1%) compared with the white population (incidence 12–15%). A previous study involving urinary prothrombin fragment 1 from both populations demonstrated superior inhibitory activity associated with the protein from the black group. In the present study, we compared N-linked and O-linked oligosaccharides released from urinary prothrombin fragment 1 isolated from the urine of healthy and stone-forming subjects in both populations to elucidate the relationship between glycosylation and calcium oxalate stone pathogenesis. The O-glycans of both control groups and the N-glycans of the black control samples were significantly more sialylated than those of the white stone-formers. This demonstrates a possible association between low-percentage sialylation and kidney stone disease and provides a potential diagnostic method for a predisposition to kidney stones that could lead to the implementation of a preventative regimen. These results indicate that sialylated glycoforms of urinary prothrombin fragment 1 afford protection against calcium oxalate stone formation, possibly by coating the surface of calcium oxalate crystals. This provides a rationale for the established roles of urinary prothrombin fragment 1, namely reducing the potential for crystal aggregation and inhibiting crystal–cell adhesion by masking the interaction of the calcium ions on the crystal surface with the renal cell surface along the nephron.

The difference in the incidence of kidney stones between South Africa's white and black populations is well documented [1,2]. In contrast to the increased incidence of urolithiasis in the Western world [3], it has been recently suggested that the incidence of kidney stones among the black population is still rare [4].

In an effort to address this observation, the possible role of urinary proteins in the black South African

Abbreviations
2AB, 2-aminobenzamide; Abs, *Arthrobacter ureafaciens* sialidase; Amf, almond meal fucosidase; Bkf, bovine kidney fucosidase; Btg, bovine testes galactosidase; CaOx, calcium oxalate; Gla, γ-carboxyglutamic acid; GU, glucose unit; HexNAc-Hex, *N*-acetyl hexosamine–hexose; Nan1, *Streptococcus pneumoniae* sialidase; NP, normal phase; Spg, *Streptococcus pneumoniae* galactosidase; THP, Tamm–Horsfall protein; UPTF1, urinary prothrombin fragment 1; WAX, weak anion exchange.

population has been investigated. Recent studies have validated this hypothesis and have implicated three urinary proteins, namely Tamm–Horsfall protein (THP), albumin and urinary prothrombin fragment 1 (UPTF1). Crystallization studies have shown that both THP [5] and albumin [6] from black subjects are better inhibitors of calcium oxalate (CaOx) crystallization than the corresponding protein from white subjects. Comparative studies of UPTF1 from white and black subjects have revealed differences in inhibitory activity with respect to crystal growth and aggregation which contribute to the protection of the black population [7].

UPTF1 is highly glycosylated but its glycans have never been fully characterized or investigated as potential role-players in stone formation, even though differences in the glycosylation of other urinary proteins from controls and stone-formers have been identified. THP [8,9] and bikunin [10] from stone-formers are less highly sialylated than the protein from controls. Furthermore, the asialo forms of THP [11,12] and bikunin [10], as well as osteopontin [13], are less efficient inhibitors of crystallization than the native glycoproteins.

Although the glycosylation of UPTF1 has not been studied, three reports have investigated oligosaccharide structures on bovine prothrombin, which is highly homologous to the human form of prothrombin from which UPTF1 is derived [14–16]. Incorporating preliminary results obtained in the two earlier studies, Mizuochi identified three biantennary, complex structures on prothrombin that were highly sialylated. Harlos *et al*. [17] produced a model of bovine protein in which two similar carbohydrate chains were located on the protein's kringle domain.

In the present study, we characterized the carbohydrate moiety of UPTF1 derived from the urine of controls and stone-formers from the white and black populations in South Africa. Differences were identified in their levels of sialylation, providing a potential diagnostic method for risk factors.

Results

N-linked glycosylation

The N-linked glycans were enzymatically released from SDS/PAGE-purified UPTF1, which ran with a characteristic relative molecular mass of 31 kDa. The fluorescently labeled (2-aminobenzamide, 2AB) glycan pool was resolved by normal phase (NP) HPLC (Fig. 1). Representative chromatograms are shown for each group, namely the white and black controls and stone-formers. The peaks are numbered in the boxed section and the corresponding assignments are shown in Table 1. The three major glycans were biantennary (A2), digalactosylated (G2) structures either asialo [A2G2, peak 12 (6%)], monosialylated [A2G2S1, peak 16 (29%)] or disialylated [A2G2S2, peak 20 (47%)] (Fig. 2). Other minor peaks, each of which comprised up to 4% of the total glycan pool, are also shown (Fig. 1, Table 1). Preliminary assignments were confirmed by a series of exoglycosidase arrays and weak anion exchange (WAX) HPLC analyses of the total glycan pool [18].

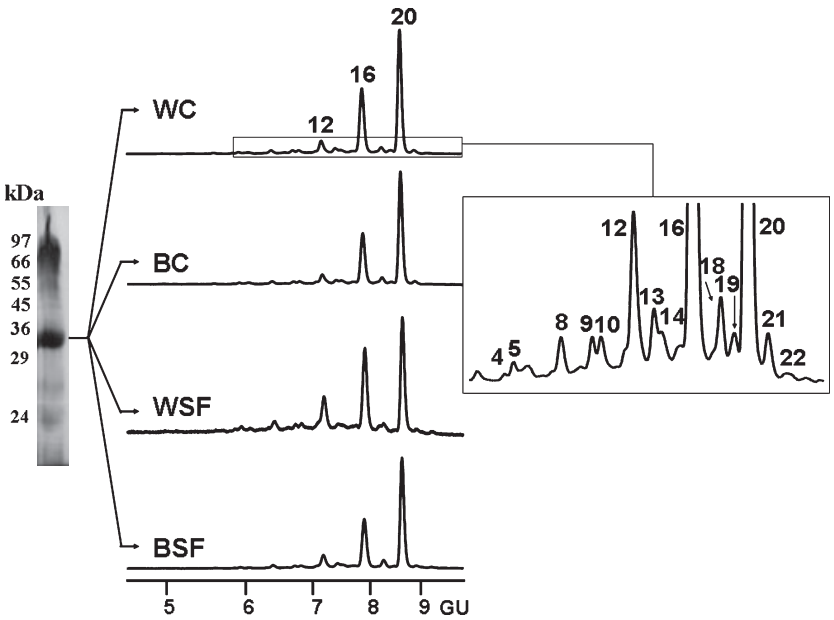

Fig. 1. SDS/PAGE showing the typical pattern of crystal matrix proteins from urine. Urinary prothrombin fragment 1 (UPTF1) is indicated by the prominent band near 36 kDa. The NP HPLC chromatograms are representative of the N-linked glycans released from UPTF1 derived from a white control subject (WC6), a black control subject (BC5), a white stone-former (WSF2) and one black stone-former (BSF). The GU values, which reflect the relative size of the glycans, are shown on the *x*-axis. The peak numbers correspond to the structures shown in Table 1.

Table 1. Analysis of N-linked glycans on urinary prothrombin fragment 1 (UPTF1). All N-glycans have two core GlcNAcs; F, fucose (FA2G2, core fucose, A2G2F, outer arm fucose); A, number of antennae (GlcNAc) on trimannosyl core; A2, biantennary; G, galactose; S, sialic acid [3], [6], the arm of the trimannosyl core to which galactose is attached; (3), (6), the sialic acid linkage; LC-ESI-MS indicates that all sialic acids are Neu5Ac.

			% Area of digestions			
Peak no.	Structure	GU	Undigested	Abs	Abs + Amf	Abs + Amf + Spg
1	A1[6]	4.90				4
2	A1[3]	5.26				2
3	A2	5.50				92
4	A1[6]G1	5.83	< 1	1	1	
5	A1[3]G1	5.90	< 1	3	2	
6	FA2	5.90				2
7	A2[6]G1	6.28		1	1	
8	A2[3]G1	6.37	2	2	2	
9	A1[6]G1S1(6)	6.70	1			
10	A1[3]G1S1(6)	6.80	2			
11	FA2G1	7.07		2	2	
12	A2G2	7.16	6	85	90	
13	A2G1FS1(6)	7.36	3			
14	A2G1S1(3)	7.49	2			
15	FA2G2	7.58		2	2	
16	A2G2S1(6)	7.88	29			
17	A2G2F	7.92		4		
18	A2G2S2(3)	8.25	3			
19	A2G2FS1(6)	8.40	2			
20	A2G2S2(6)	8.56	47			
21	A2G2FS2(6)	8.91	2			
22	FA2G2S2(6)	9.26	< 1			

Abs, *Arthrobacter ureafaciens* sialidase; Amf, almond meal α-fucosidase; Spg, *Streptococcus pneumoniae* β-galactosidase.

Figure 2 shows the NP HPLC profiles of the total glycan pool of WC6 together with representative exoglycosidase digestions with α2–3,2–6 sialidase (*Arthrobacter ureafaciens* sialidase, Abs), α1–3,4 fucosidase (almond meal fucosidase, Amf) and β1–4 galactosidase (*Streptococcus pneumoniae* galactosidase, Spg). The corresponding percentage peak areas are presented in Table 1. Digestion with α2–3 sialidase (*Streptococcus pneumoniae* sialidase, Nan1) indicated that peaks 14 and 18 contained α2–3 linked sialic acid residues (data not shown). Fucose substitution on both the core GlcNAc and the GlcNAc on the 6-antenna of A2G2 were detected by negative ion nanospray MS/MS [19]. The presence of core fucose was confirmed by digestion with bovine kidney fucosidase, which converted FA2G2S2 (peak 22) to A2G2S2 (data not shown). However, A2G2FS2 (peak 21) was not affected by treatment with bovine kidney fucosidase and was

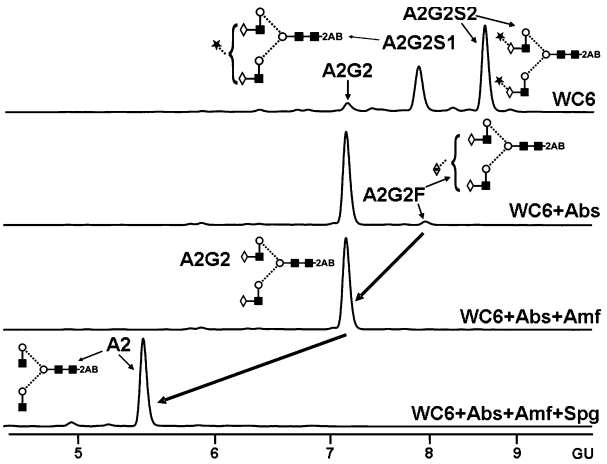

Fig. 2. NP HPLC chromatograms of the N-linked glycans released from the white control subject (WC6) following arrays of exoglycosidase digestions. Structures labeled on the top profile are present in the undigested glycan pool at over 6%. See Table 1 for percentage peak areas. Exoglycosidase abbreviations: Abs, *Arthrobacter ureafaciens* sialidase; Amf, almond meal α-fucosidase; Spg, *Streptococcus pneumoniae* β-galactosidase. See Table 5 for an explanation of the symbols used in the structures.

digested to A2G2 with Abs and almond meal fucosidase, identifying the fucose as outer arm α1–3 linked to GlcNAc. The assignments of the major peaks were consistent with data from MALDI-TOF MS, negative ion nano-ESI MS, MS/MS and LC positive ion ESI/MS/MS (Table 2).

Analysis of glycans by charge

The total glycan pool was separated into neutral, monosialylated and disialylated fractions by WAX HPLC (Fig. 3A); each of these fractions was then analysed by NP HPLC (Fig. 3B). More than 90% of the N-linked glycans were confirmed as monosialylated and disialylated structures. The same N-linked structures were observed in all four groups investigated but they varied in their proportions.

Further analysis of all of the N-linked glycan samples was carried out with respect to sialylation. Comparisons between white controls and white stone-formers and between black controls and black stone-formers did not reveal significant differences in the sialylation of these groups. Although another obvious comparison would have been between black controls and black stone-formers, our solitary subject in the latter group precluded a meaningful interpretation. Of interest is the comparison between black controls and white stone-formers, as these groups represent the two extremes of the stone formation risk spectrum. Indeed, our observation of a significant difference in the

Table 2. Mass data of N-linked glycans on urinary prothrombin fragment 1 (UPTF1). FA2G2S2 also observed as monosialylated and desialylated structures, as sialic acid residues frequently decompose on MALDI-TOF MS. ND, not detected.

	MALDI-TOF MS m/z ($[M + Na]^+$)		LC-ESI MS m/z ($[M + 2H]^+$)		Nano-ESI MS[c] m/z $[M - H]^-$ ($[M + H_2PO_4]^-$)		Composition			
Structure[a]	Obs.	Calc.	Obs.[b]	Calc.	Obs.	Calc.	Hex	HexNAc	Neu5Ac (Na)	Fucose
A1	1256.6	1256.5	ND	617.7	1210.4	1210.4	3	3	0	0
A1G1	1418.6	1418.5	ND	698.8	1372.5	1372.5	4	3	0	0
A2G1	1621.7	1621.6	ND	800.3	1575.5	1575.5	4	4	0	0
A1G1S1	1731.6	1731.6	925.3	925.4	1685.6	1685.6	4	3	1	0
A2G2	1783.6	1783.7	881.2	881.3	1737.6	1737.6	5	4	0	0
FA2G2	1929.9	1929.7	ND	954.4	1883.6	1883.6	5	4	0	1
A2G2S1	2096.6	2096.7	1026.9	1026.9	2050.7	2050.7	5	4	1	0
FA2G2S1	2242.8	2242.8	ND	1099.9	ND	2196.8	5	4	1	1
A2G2S2	2409.6	2409.8	1172.3	1172.4	2363.8	2363.8	5	4	2	0
FA2G2S2	2555.1	2555.9	1245.5	1245.5	ND	2508.9	5	4	2	1

[a] Refer to Table 1 for structure abbreviations. [b] Also detected as monosodium and disodium adducts. [c] Neutral glycans produce $[M + H_2PO_4]^-$ ions, whereas the sialylated glycans yield $[M - H]^-$ under the conditions used.

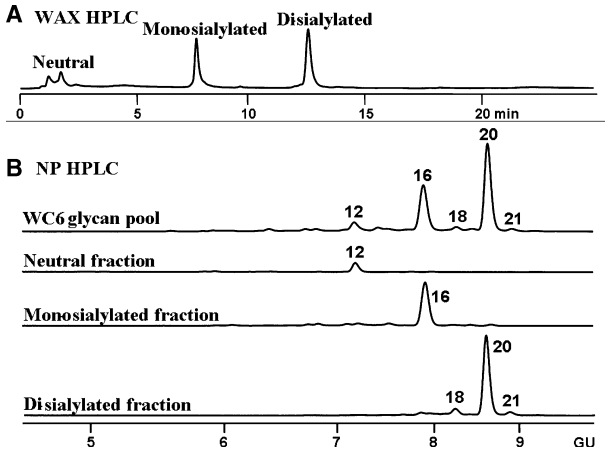

Fig. 3. HPLC analysis of N-linked glycans released from urinary prothrombin fragment 1 (UPTF1). These glycans were separated into neutral, monosialylated and disialylated fractions by WAX HPLC (A), and then the fractions were analyzed by NP HPLC (B). See Table 1 and Fig. 1 for peak numbers.

respective sialylation of UPTF1 in the latter two groups bears testimony to a possible link between the degree of sialylation and stone risk.

Table 3 shows the percentage of the monosialylated and disialylated fractions and the ratio of the two fractions, together with the averages and standard errors for white controls, black controls and white stone-formers. The ratio of monosialylated/disialylated residues varied between these groups. The white stone-formers had a significantly lower ratio than the black control group ($P = 0.007$). This indicates that, in the black control group, N-linked glycans present a greater number of negatively charged sialic acid residues by virtue of their greater proportion of disialylated structures.

Moreover, significant differences emerged when a comparison of the three groups white controls, black controls and white stone-formers was also made by calculating the maximum potential sialylation for UPTF1 from each individual. This value was based on the percentage of monoantennary and biantennary structures, which all have the potential to be galactosylated and sialylated in the Golgi glycosylation processing pathway on one or both arms. The level of sialylation that was detected was then compared to the calculated maximum potential sialylation, i.e. total (actual) sialylation compared with potential sialylation expressed as a percentage (Table 4). The percentages in the three groups are shown graphically in Fig. 4. The black control group had a significantly higher mean percentage of actual/potential sialylation than the white stone-formers ($P = 0.002$). All of the white stone-formers had actual/potential sialylation at or below 72%. The majority of the white stone-formers had values below 65%. In contrast, the black controls all had values above 69%, with the majority of these being above 72%. The white controls had the largest variation (between 64% and 80%). In both control groups there were samples with sialylation values below 72%, which may indicate the risk of an individual developing kidney stones.

O-linked glycosylation

NP HPLC chromatograms of the undigested O-linked glycans from pooled samples of white and black

Table 3. Percentage of monosialylated and disialylated N-linked glycans on urinary prothrombin fragment 1 (UPTF1) from white control subjects (WC) and black control subjects (BC), white stone-formers (WSF) and a black stone-former (BSF). Monosialylation, disialylation and total sialylation: all *P*-values > 0.05. Monosialylation/disialylation ratio: WC versus BC $P > 0.05$, WC versus WSF $P > 0.05$, BC versus WSF $P = 0.007$.

Sample	Monosialylation	Disialylation	Total sialylation	Monosialylation/ disialylation
WC1	42.8	40.5	83.3	1 : 0.95
WC2	33.9	56.7	90.6	1 : 1.67
WC3	28.9	64.3	93.2	1 : 2.22
WC4	44.5	38.7	83.3	1 : 0.87
WC5	44.7	38.5	83.2	1 : 0.86
WC6	38.7	51.4	90.2	1 : 1.33
WC7	41.7	41	82.7	1 : 0.98
WC8	33.3	58.6	91.9	1 : 1.76
WC average ± SE	38.5 ± 2.1	48.7 ± 3.6	87.3 ± 1.6	1 : 1.33
BC1	35.2	54.8	90	1 : 1.56
BC2	36.3	54.8	91.1	1 : 1.51
BC3	33	59.1	92.1	1 : 1.79
BC4	28.8	65.7	94.5	1 : 2.28
BC5	36.1	53.6	89.7	1 : 1.48
BC6	34.5	51.8	86.3	1 : 1.50
BC7	36.2	45.6	81.8	1 : 1.26
BC average ± SE	34.3 ± 1.0	55.1 ± 2.4	89.3 ± 1.6	1 : 1.62
WSF1	38.3	49.9	88.2	1 : 1.30
WSF2	43.1	35.6	78.7	1 : 0.82
WSF3	35.6	49.7	85.3	1 : 1.40
WSF4	44.7	38.6	83.3	1 : 0.86
WSF5	45.2	38.8	83.9	1 : 0.86
WSF6	43.8	39.1	82.9	1 : 0.89
WSF average ± SE	41.8 ± 1.6	41.9 ± 2.5	83.7 ± 1.3	1 : 1.02
BSF	34.9	53.9	88.8	1 : 1.54

control subjects and white stone-formers are shown in Fig. 5. The corresponding structures, as well as their percentage peak areas, are presented in Table 5. Peak m (an α2-6 sialylated unidentified structure) was present in both control groups but absent in the stone-formers. Peaks p and q (sialylated Galβ1-4 HexNAc-Hex structures) were only detected in low amounts on the NP HPLC (with the greatest proportion in the control samples) and were only detected by MS in the controls. The latter two structures are unusual O-glycan structures which we have shown to be α2–3 and α2–6 sialylated Galβ1–4 HexNAc-Hex structures by sequential exoglycosidase digestions (Fig. 6), LC-ESI-MS (Table 6) and ESI-MS/MS (Fig. 7). The most probable structures contain core GlcNAc-mannose linked to Ser/Thr. These have been previously identified in mammalian brain, nerve and skeletal muscle [20]. This epitope is also found on N-glycans, so there is the possibility that this tetrasaccharide is a degradation product from N-glycans. However, this is unlikely, as all of the samples analysed, including bovine serum fetuin, contained N-glycans with this epitope, but the O-glycan tetrasaccharide was only detected in the control UPTF1 samples.

Eight of the nine O-glycan structures with two or more monosaccharides were identified on the basis of their relative retention times on NP HPLC in comparison with a bovine fetuin standard released at the same time and an O-link structure database [21]. One of the nine O-glycan structures, at glucose unit (GU) 0.90, has only one monosaccharide. The assignments were confirmed by data obtained from an array of exoglycosidase digestions (Fig. 6), LC-ESI and both negative and positive ion nanospray MS (Table 6, Fig. 7). The O-glycans of UPTF1 consist of Galβ1-3GalNAc core (core 1), GlcNAcβ1-6(Galβ1–3)GalNAc core (core 2) or HexNAc-Hex (possibly GlcNAc-mannose) with additional galactose β1-4 and/or sialic acids α2-3 and/or α2-6. A high proportion of the glycans were sialylated and these proportions differed between the control and stone-forming groups: white controls, 41.3%; black controls, 38.2%; and white stone-formers, 25.0%.

The results of the LC-ESI-MS fragmentation analysis of the white control and white stone-former O-glycan

Table 4. Calculation of sialylated galactose residues of N-glycans on urinary prothrombin fragment 1 (UPTF1) from white control (WC) and black control (BC) subjects, white stone-formers (WSF) and a black stone-former (BSF) as a percentage of the maximum potential sialylation of one sialic acid per galactose. WC versus BC $P > 0.05$, WC versus WSF $P > 0.05$, BC versus WSF $P = 0.002$.

Sample	Maximum potential sialylation [a]	Monosialylation (%area x1)	Disialylation (%area x2)	Total (actual) sialylation	% Actual/potential sialylation [b]
WC1	193	42	81	123	63.9
WC2	195	34	113	147	75.4
WC3	196	29	129	157	80.3
WC4	190	45	77	122	64.3
WC5	190	45	77	122	64.1
WC6	194	39	103	142	72.8
WC7	191	42	82	124	64.7
WC8	196	33	117	150	76.7
WC average ± SE					70.3 ± 2.4
BC1	195	35	110	145	74.2
BC2	195	36	110	146	74.9
BC3	194	33	118	151	78.1
BC4	197	29	131	160	81.2
BC5	192	36	107	143	74.8
BC6	190	34	104	138	72.6
BC7	184	36	91	127	69.1
BC average ± SE					75.0 ± 1.5
WSF1	193	38	100	138	71.6
WSF2	189	43	71	114	60.6
WSF3	191	36	99	135	70.7
WSF4	191	45	77	122	63.8
WSF5	191	45	78	123	64.2
WSF6	190	44	78	122	64.4
WSF average ± SE					65.9 ± 1.8
BSF	195	35	108	143	73.2

[a] Derived from percentage areas of (monoantennary + 2 × biantennary) glycans in each sample. [b] % Actual/potential sialylation = (total sialylation/maximum potential sialylation) × 100.

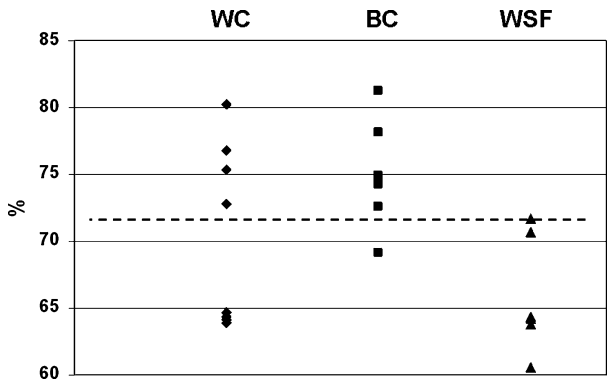

Fig. 4. Percentage potential sialylation of N-linked glycans released from urinary prothrombin fragment 1 (UPTF1) for individual samples from white controls, black controls and white stone-formers. The dotted line indicates the maximum value observed in the white stone-formers for the N-linked glycans.

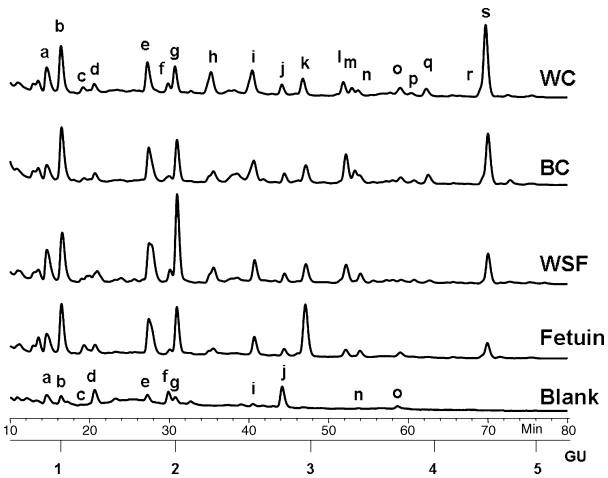

Fig. 5. NP HPLC analysis of O-linked glycans released from urinary prothrombin fragment 1 (UPTF1) derived from white (WC) and black (BC) control subjects and white stone-formers (WSF). The percentage peak areas of the digests and the structures corresponding to each letter are shown in Table 5.

pools, which were used to confirm the exoglycosidase digestion sequencing data, are presented in Table 6. Seven of the nine structures were also identified using

Table 5. Analysis of O-linked glycans on urinary prothrombin fragment 1 (UPTF1). Bgd, background peaks detected in blank run; ND, not detected.

Peak ID[a]	Structure[b]	GU	% Area WC	BC	WSF
a	2AB + bgd	0.90	7.0	4.0	8.7
b	Hexose + Bgd	1.00	12.2	14.6	13.2
c	Bgd	1.18	1.4	1.2	1.0
d	Bgd	1.27	2.5	2.6	3.2
e	2AB + bgd	1.73	8.8	10.8	15.2
f	Bgd	1.91	2.1	1.4	2.7
g[c]	Bgd	1.97	6.7	10.2	20.9
h[d]	2AB	2.27	7.0	4.4	5.2
i	Bgd	2.60	8.5	7.4	5.0
j	Bgd	2.82	2.7	2.2	2.0
k	2AB	2.98	4.8	5.0	4.6
l	2AB	3.29	4.2	9.0	5.8
m	Neu5Ac α2–6-?	3.35	2.2	3.5	ND
n	Bgd	3.40	1.4	2.0	2.7
o	Bgd	3.72	3.3	1.9	0.4
p	2AB	3.81	1.1	0.9	0.6
q	2AB	3.93	2.6	2.9	0.7
r	2AB	4.45	21.7	16.1	8.1
s	2AB	4.45	21.7	16.1	8.1

GalNAc; Gal; NeuNAc; GlcNAc; Unknown Hexose; Unknown HexNAc;

Linkage position

6 8 4 3 2

β linkage
α linkage
Unknown β-Linkage
Unknown α-Linkage

[a] Peak ID labels in Fig. 3. [b] Structures determined by GU comparison with database [21] before and after exoglycosidase digestions (see Fig. 6), LC-MS and ESI-MS/MS data (Table 6 and Fig. 7). [c] This peak is predominantly background lactose. [d] This structure is a 'peeled' product resulting from breakdown of glycans during hydrazinolysis.

these data. LC-ESI-MS also indicated that considerably more of the core 1 structure was present in white stone-formers than in white controls (data not shown).

Molecular model of urinary prothrombin fragment 1

A molecular model of UPTF1 (Fig. 8) was generated using the calcium-bound bovine prothrombin fragment 1 crystal structure along with predicted N-glycan and

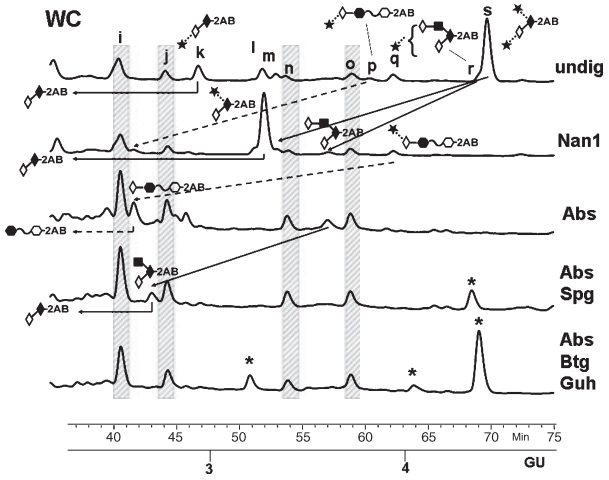

Fig. 6. NP HPLC analysis of O-linked glycans released from urinary prothrombin fragment 1 (UPTF1) of white control subjects following an array of exoglycosidase digestions. The percentage peak areas of the digests are shown in Table 5. Exoglycosidase abbreviations: Nan1, *Streptococcus pneumoniae* sialidase; Abs, *Arthrobacter ureafaciens* sialidase; Spg, *Streptococcus pneumoniae* β-galactosidase; Btg, bovine testes β-galactosidase; Guh, *Streptococcus pneumoniae* glucosaminidase. Shaded areas indicate background peaks. Peaks marked with asterisks originate from N-glycans present in the glycan pool.

O-glycan sites. The three-dimensional structure is composed of a kringle domain and a Gla domain (Fig. 8A). In the latter, seven calcium atoms are bound to γ-carboxyglutamic acid residues (or Gla residues). Based on steric constraints, both of the predicted N-glycan sites (Asn78 and Asn100) and two of the five predicted O-glycan sites (Thr121 and Thr122, but not Thr102, Ser120 and Thr149) were occupied (SWISS-PROT numbering P00734; Ala44 corresponds to PDB structure Ala1). The four occupied glycan sites are all located on the kringle domain. An A2G2S2 N-glycan structure and a monosialylated core 1 O-glycan structure were used to represent the identified glycans in the model, since these structures constituted significant proportions of the N-glycan and O-glycan pools, respectively. The distances between adjacent glycan chains are 40 Å and 43 Å for O–N and 60 Å for N–N (Fig. 8B). Moreover, the diameter of the glycoprotein (63 Å) was significantly increased compared with its unglycosylated form (36 Å).

Discussion

O-linked glycosylation

The O-glycans of UPTF1 consist of core 1 and core 2 structures, and an unusual glycan with a HexNAc-

Table 6. O-Glycans detected on urinary prothrombin fragment 1 (UPTF1) derived from white controls (WC) and stone-formers (WSF) by LC-ESI-MS. ND, not detected. The $Hex_2{\cdot}Hex{\cdot}NAc_1{\cdot}Neu5{\cdot}Ac_1$ mass was not detected in the white stone-former (WSF) or the fetuin control O-glycan release, which was run at the same time. Therefore, this is a real O-glycan peak and is not a degradation product from N-glycans that are present on all of the glycoproteins studied. Fragmentation patterns from the other glycans listed in this table were all consistent with the listed structures (data not shown).

		Mass				Composition					
		Observed								Retention	
Peak ID	Structure	WC	WSF	Calc.	Adduct	Hex	HexNAc	NeuNAc	2AB	time (min)[a]	GU[b]
e		504.14	504.14	504.22	$[M + H]^+$	1	1	0	1	44.8	1.8
		526.11	526.11	526.20	$[M + Na]^+$						
h[c]		592.15	592.15	592.24	$[M + H]^+$	1	0	1	1	48.7	2.3
		614.13	614.13	614.22	$[M + Na]^+$						
k and l	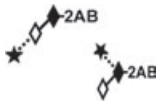	795.21	795.21	795.32	$[M + H]^+$	1	1	1	1	58.1 and 59.1	3.0 and 3.3
		817.25	817.25	817.30	$[M + Na]^+$						
p and q	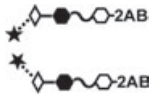	957.26	ND	957.37	$[M + H]^+$	2	1	1	1	63.4	3.8 and 3.9
		979.25	ND	979.35	$[M + Na]^+$						
s		1086.27	1086.27	1086.41	$[M + H]^+$	1	1	2	1	65.5	4.4
		1108.25	1108.25	1108.39	$[M + Na]^+$						

[a] Retention time on LC-MS micro 2 × 250 mm column. [b] This is the GU value from the 4.6 × 250 mm column. [c] Peeled product.

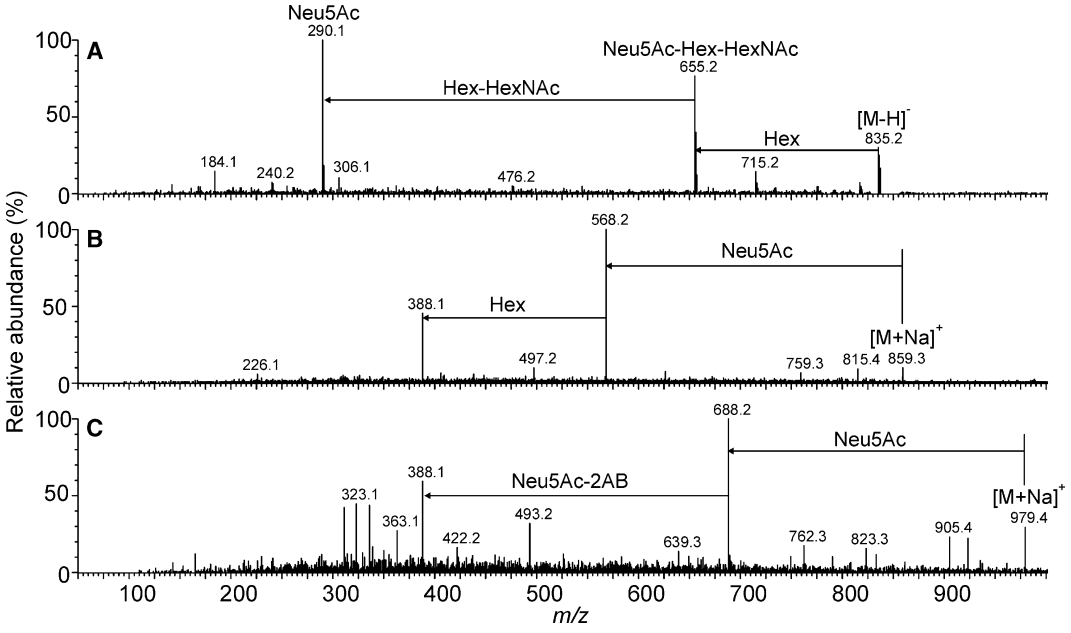

Fig. 7. Mass data of O-linked glycans released from urinary prothrombin fragment 1 (UPTF1) of white control (WC) subjects. (A) Negative ion nanospray MS/MS spectrum of the $[M - H]^-$ ion (*m/z* 835) from the $Hex_2{\cdot}Hex{\cdot}NAc_1{\cdot}Neu_5{\cdot}Ac_1$ glycan (peak q). The ion at *m/z* 306.1 is indicative of an α2–6-linked sialic acid. (B) Positive ion MS/MS spectrum of the $[M + Na]^+$ ion (*m/z* 859) from the $Hex_2{\cdot}Hex{\cdot}NAc_1{\cdot}Neu_5{\cdot}Ac_1$ glycan. (C) Positive ion fragmentation pattern of the $[M + Na]^+$ ion (*m/z* 979) from the 2-aminobenzamide (2AB) derivative of the $Hex_2{\cdot}Hex{\cdot}NAc_1{\cdot}Neu_5{\cdot}Ac_1$ glycan. The predominant ions are *m/z* 688 from loss of terminal sialic acid, and *m/z* 388 [Hex-HexNAc + Na]$^+$, which is consistent with further loss of hexose-2AB.

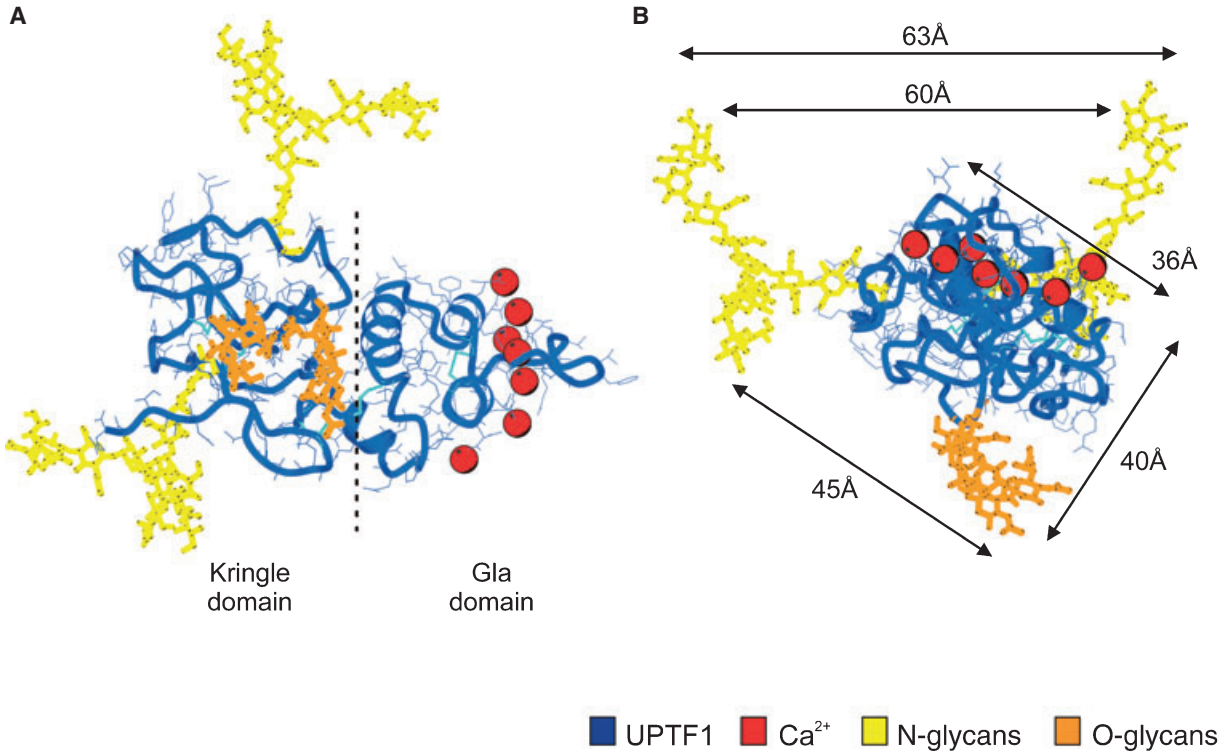

Fig. 8. Molecular model of urinary prothrombin fragment 1 (UPTF1). (A) Side-on view showing the two protein domains. (B) End-on view down the Gla domain.

Hex core (possibly GlcNAc-mannose) and additional galactose β1–4 and/or sialic acids α2–3 and/or α2–6. The O-glycans from the control groups were more highly sialylated (white controls 41.3%, black controls 38.2%) than those from the white stone-formers (25.0%). The controls also contain a higher proportion of glycans with the HexNAc-Hex core (3.7% and 3.8% for white controls and black controls, respectively, compared to 1.3% for white stone-formers).

N-linked glycosylation

Complex biantennary N-linked glycans with up to ~90% sialylation, were found on UPTF1 from both healthy and stone-forming subjects. The sialic acid residues were α2–3 and α2–6 linked to galactose residues, which were all β1–4 linked. Core and outer arm fucosylation was observed. The black control group had a significantly greater ratio of monosialylated/disialylated structures (1 : 1.62 versus 1 : 1.02) as well as a significantly greater percentage of potential sialylation (75.0% versus 65.9%) than the white stone-formers. The identification of sialylated A2G2 structures (~ 76% of total N-linked glycan pool) is consistent with a previous study of bovine prothrombin, which demonstrated extensive sialylation of the glycoprotein with sialic acids on both Gal and GlcNAc residues [16]. Mizuochi reported α2–6-linked sialic acids with β1–4-linked galactose and α2–3-linked sialic acids with β1–3-linked galactose on bovine prothrombin. This reflects the species-specific nature of glycosylation processing.

Significant differences in sialylation have implications for stone formation

The O-glycans of both control groups were significantly more sialylated than those of the white stone-formers. Fifty per cent of N-glycans from white control samples (i.e. four of eight) and 86% of the black controls (i.e. six of seven) were significantly more sialylated than those from the white stone-formers. Both control groups also contained UPTF1 samples with low sialylation within the range of the stone-formers (50% of the white group and 14% of the black group), suggesting a predisposition to kidney stones. While stone formation [22] and the recurrence [23] thereof varies with age, studies have not addressed the question of whether sialylation might also be affected. Although these factors could have influenced our results, we suggest that our observed differences in sialylation are associated with different risk profiles for

kidney stone formation. Our results indicate that the N-linked and O-linked glycans in most of the control samples present a greater negative charge on UPTF1 than in the stone-formers by virtue of their enhanced sialylation. This has two implications for inhibition of stone formation, namely decreases in the tendencies for crystal aggregation and crystal–cell adhesion.

Crystal aggregation

Crystal aggregation is largely influenced by the surface properties of crystals. The binding of proteins to crystal surfaces results in a more negative electrostatic potential (or zeta potential), which in turn increases the electrostatic repulsive forces between crystals and decreases their tendency to aggregate [24]. In fact, oxidatively modified THP loses its zeta potential [25] and this has been linked to a decrease in the sialic acid content of the protein [9]. Thus it is likely that the more highly sialylated UPTF1 from black control subjects results in less crystal aggregation than UPTF1 from white stone-formers.

The kringle domain of UPTF1

Molecular modeling located two N-glycans and two O-glycans on the kringle domain of UPTF1. Glycosylation influences the inhibitory properties of several urinary proteins [10–13], and it is therefore probable that the kringle domain of UPTF1 contributes to its activity. This is noteworthy because it is the Gla domain that reportedly imparts the inhibitory potency of the protein by way of its binding to calcium ions [26].

Interaction of CaOx crystals with renal cell surfaces

Concomitant with their effect on inhibitory activity, the glycans, and in particular sialic acids, may play a role in mediating crystal interactions with renal epithelial cells. Several studies have reported the binding of CaOx crystals to renal cell surfaces [27–30], and this is now widely regarded as a possible mechanism of stone formation, in addition to blockage of the nephron by aggregates of CaOx crystals [31].

Whereas renal cells present a negatively charged surface [30], CaOx crystals exhibit a positive character, due to the proximity of their calcium ions to the crystal surface. Induction of a negative charge on the crystal surface by proteins would reduce crystal adhesion to the renal cell surface by way of electrostatic repulsion. A recent study demonstrated that UPTF1 reduces crystal adhesion by coating the surface of exogenous CaOx monohydrate crystals in the presence of whole urine [32]. It is possible that Kumar's observation was directed in part by the presence of highly sialylated glycans on UPTF1.

Terminal sialic acids contribute largely to the negative character of the renal cell surface [33], and several studies have focused on this sugar. Sialic acid-containing cell surface glycoproteins are critical determinants of crystal binding, since pretreatment of cells with neuraminidase greatly reduces CaOx monohydrate crystal binding [31]. Sialic acids also direct the face-selective nucleation of CaOx dihydrate crystals onto renal epithelial cell surfaces [34]. It is apparent that sialic acids play an important role in the attachment of CaOx crystals to renal cells; however, the aforementioned studies have focused on the role of cell surface glycans rather than crystal-associated ones, which may also be expected to play a significant role in crystal–cell adhesion.

Conclusion

The present study has shown a correlation between sialylation and disease, and the glycosylation of UPTF1 provides an important rationale for the retardation of CaOx crystal aggregation and blocking the adhesion of CaOx crystals to renal cells. The distribution of the percentages of sialylated UPTF1 glycans across the three groups also reveals a risk factor among controls. Genetic factors may contribute to the differences in the sialylation of UPTF1, particularly between the black control group and white stone-formers. While there are differences in glycosylation between controls and stone-formers, there are overlaps in, for example, the maximum potential sialylation of N-linked glycans. Therefore, our results provide the promise of an additional diagnostic tool to be used in conjunction with other tools such as urinary supersaturation [35], which is also not a foolproof discriminator [36]. The difference in sialylation between the two groups suggests a protective role for the glycans among the black population and provides a basis for testing a larger group of individuals to determine whether this will provide a robust diagnostic risk factor marker.

Experimental procedures

Protein preparation

CaOx crystals were precipitated from 24 h urine samples, and the proteins from the crystal matrix extract **[7]** were

used for the N-glycan study. Crystals were prepared from the following sources: urine samples from eight healthy white males and seven healthy black males (aged 20–30 years), and urine samples from six white male CaOx stone-formers and one black male CaOx stone-former (aged 40–65 years). All subjects except for one white stone-former fell within the age range 20–60 years specified by Hesse *et al*. [22] as appropriate for comparison between healthy and stone-forming males. All of the stone-formers had either passed a stone or had one surgically removed during the 9 months prior to commencement of the study.

Purified UPTF1 (38 μg) from three or more pooled urine samples (to ensure adequate quantities) of healthy white and black males and white CaOx stone-formers was used for analysis of the O-linked glycans. The purification procedure has been described in detail elsewhere **[7]**. Briefly, crystal matrix proteins were prepared as for the N-glycan study, and UPTF1, the major protein included therein, was isolated using reverse-phase HPLC. Insufficient UPTF1 from black stone-formers was available for the analysis of O-linked glycans.

UPTF1 purified by crystal precipitation is representative of UPTF1 in the urine. It has been shown that at high levels of CaOx supersaturation, such as those used to precipitate crystals from which UPTF1 was isolated, at least 80% of UPTF1 is attached to urinary crystals [37]. This therefore represents a significant proportion of the total UPTF1 in urine and not merely a subpopulation.

Release and fluorescent labeling of glycans

For the analysis of N-linked glycans, approximately 12 μg of crystal matrix proteins were loaded onto 12.5% polyacrylamide minigels and visualized using Coomassie Brilliant Blue. The bands corresponding to UPTF1 (major band at ~31 kDa) were excised and the N-glycans were released by *in situ* deglycosylation with peptide N-glycanase F (Roche Diagnostics, GmbH Mannheim, Germany) as previously described [38,39]. O-linked glycans were released from purified UPTF1 samples by manual hydrazinolysis [21]. The released glycans were then fluorescently labeled with 2AB (Ludger Ltd, Abingdon, UK).

NP HPLC

Aliquots of the glycan pools were analyzed by NP HPLC using a 4.6×250 mm TSK gel Amide-80 column (Anachem, Luton, UK) with the low salt buffer system previously described [18]. A 2AB-labeled dextran hydrolysate ladder standard consisting of glucose oligomers was used to calibrate the system. The number of glucose residues (GU units) of the dextran peaks was used to calculate the GU value of the unknown glycan structures for comparison with a database of known structures. Preliminary assignments were then made on the structure of each glycan peak and the area of each peak was calculated and expressed as a percentage of the total glycan pool.

Exoglycosidase digestions

Aliquots of the N-linked and O-linked glycan pools were incubated overnight with arrays of exoglycosidases at 37 °C and then subjected to NP HPLC. The following enzymes, obtained from Prozyme (San Leandro, CA, USA), were used in various combinations: *Arthrobacter ureafaciens* sialidase (Abs, EC 3.2.1.18) (1 $U \cdot mL^{-1}$), which removes both α2–3-linked and α2–6-linked sialic acids; *Streptococcus pneumoniae* sialidase recombinant in *Escherichia coli* (Nan1, EC 3.2.1.18) (1 $U \cdot mL^{-1}$), which only removes α2–3-linked sialic acids; almond meal α-fucosidase (Amf, EC 3.2.1.111) (2 $mU \cdot mL^{-1}$), which removes outer arm α1–3-linked and α4-lnked fucose; bovine kidney α-fucosidase (Bkf, EC 3.2.1.51) (1 $U \cdot mL^{-1}$), which removes core α1–6-linked fucose; bovine testes β-galactosidase (Btg, EC 3.2.1.23) (1 $U \cdot mL^{-1}$), which removes both β1–3-linked and β1–4-linked galactose; *Streptococcus pneumoniae* β-galactosidase (Spg, EC 3.2.1.23) (80 $mU \cdot mL^{-1}$), which removes β1–4-linked galactose only; *Streptococcus pneumoniae* glucosaminidase (EC 3.2.1.30) (4.5 $U \cdot mL^{-1}$), which removes GlcNAc only; Jack bean β-*N*-acetylhexosaminidase (EC 3.2.1.30) (50 $mU \cdot mL^{-1}$), which removes GlcNAc and GalNAc; and Jack bean α-mannosidase (EC 3.2.1.24) (50 $U \cdot mL^{-1}$), which removes α1–2-linked, α3-linked and α6-linked linked mannose residues. Following digestion, enzymes were removed using protein-binding Micropure-EZ filters (Millipore, Watford, UK).

WAX HPLC

Glycan pools were separated according to charge by WAX HPLC using a Vydac 301VHP575 column (7.5×50 mm) (Anachem Limited) [41]. Fractions were collected and analyzed by NP HPLC, and these profiles were compared with the total glycan pool obtained on NP HPLC. An aliquot of the glycans was also analyzed by WAX HPLC following overnight digestion with Abs.

MS

MALDI-TOF mass spectra of 2AB-labeled N-linked glycans were recorded using a Micromass TofSpec 2E reflection TOF mass spectrometer (Waters-Micromass Ltd, Manchester, UK) with a saturated solution of 2,5-dihydroxybenzoic acid in acetonitrile as the matrix [42].

LC-ESI-MS was performed using an LC packings Ultimate HPLC equipped with a Famos autosampler (Dionex Ltd, Camberley, UK) interfaced with a Q-Tof Ultima Global mass spectrometer (Waters-Micromass). Chromatographic separation was achieved using a 2×250 mm,

microbore NP HPLC TSK gel Amide-80 column (Hichrom, Theale, UK) with the same gradient and solvents as used with the standard NP HPLC but at a lower flow rate of 40 $\mu L \cdot min^{-1}$. The mass spectrometer was operated in positive ion mode with: 3 kV capillary voltage; RF-1 lens 60; source temperature, 100 °C; desolvation temperature, 150 °C; cone gas flow, 50 $L \cdot h^{-1}$; and desolvation gas flow, 450 $L \cdot h^{-1}$ [21].

Nano-ESI-MS/MS data were also obtained using the Q-Tof Ultima Global mass spectrometer. Samples in water/methanol (1 : 1, v/v, 5 μL) were infused with Proxeon (Proxeon Biosystems, Odense, Denmark) capillaries. Operating conditions were: capillary potential, 1.2 kV; ion source temperature, 120 °C; desolvation gas, nitrogen at 50 $L \cdot h^{-1}$; RF-1 lens, 180 V; collision gas, nitrogen at 0.5 bar; and a collision cell voltage appropriate to the mass of the ions being analyzed. Spectra of the N-linked glycans before and after desialylation (1% acetic acid, 80 °C for 30 min) were obtained in negative ion mode, whereas those of the O-linked glycans were obtained in both positive and negative ion modes. Data acquisition and processing were conducted with MASS-LYNX 4 software (Waters-Micromass).

Statistical analysis

Data analysis of the N-linked glycan samples for white controls, black controls and white stone-formers with respect to sialylation is presented as average values ± standard error (SE). The average values of the white control, black control and white stone-former groups were compared statistically by analysis of variance, with the exception of the monosialylated/disialylated ratios. Since ratios are not normally distributed, they were compared using the non-parametric Mann–Whitney *U*-test. Results were considered statistically significant if $P = 0.05$. Data for the single black stone-former were not included in the statistical analyses. All analyses were carried out using STATISTICA 7.

Molecular modeling

Molecular modeling was performed on a Silicon Graphics Fuel workstation using INSIGHTII and DISCOVER software (Accelrys, San Diego, CA, USA). The figures were produced using the programme MOLSCRIPT [43]. Since UPTF1 is an intracrystalline urinary protein, the calcium-bound bovine prothrombin fragment 1 crystal structure was used as the basis for modeling (PDB code: 1NL1). The bovine (SWISSPROT, P00735, residues 44–199) and human (SWISSPROT, P00734, residues 44–198) sequences were aligned using BLAST (http://www.ncbi.nlm.gov/BLAST). N-linked and O-linked glycan sites were generated using the database of glycosidic linkage conformations and *in vacuo* energy minimization to relieve unfavorable steric interactions. Predicted N-glycan and O-glycan sites were generated using http://www.cbs.dtu.dk/services/NetNGlyc/ and http://www.cbs.dtu.dk/services/NetOGlyc/, respectively. The Asn-GlcNAc linkage conformations were based on the observed range of crystallographic values, the torsion angles around the Asn Cα–Cβ and Cβ–Cγ bonds then being adjusted to eliminate unfavorable steric interactions between the glycans and the protein surface.

Acknowledgements

The authors (University of Cape Town) would like to record their thanks to the following organizations for funding: Harry Oppenheimer Trust, Investec South Africa, South African Medical Research Council, South African National Research Foundation, the Volkswagen Stiftung and the University of Cape Town. The glycan analysis was funded by the Oxford Glycobiology Institute Endowment, and the MS analysis was supported by grants from BBSRC and the Wellcome Trust.

References

1 Modlin M (1967) The aetiology of renal stone: a new concept arising from studies on a stone-free population. *Ann R Coll Surg Eng* **40**, 155–178.
2 Whalley NA, Moraes MFBG, Shar TG, Pretorius SS & Meyers AM (1998) Lithogenic risk factors in the urine of black and white subjects. *Br J Urol* **82**, 785–790.
3 Robertson WG (2004) The economics and epidemiology of urolithiasis. In *Kidney Stones: Inside and Out* (Gohel MDI & Au DWT, eds), pp. 368–371. Hong Kong Polytechnic University, Hong Kong.
4 Whalley NA, Martins MC, Van Dyk RC & Meyers AM (1999) Lithogenic risk factors in normal black volunteers, and black and white recurrent stone formers. *Br J Urol* **84**, 243–248.
5 Craig T-A, Rodgers AL & Brandt W (2001) Inhibition of calcium oxalate (CaOx) crystallisation by Tamm–Horsfall mucoprotein (THM) from two different population groups. In *Eurolithiasis: 9th European Symposium on Urolithiasis* (Kok DJ, Romijn HC, Verhagen PCMS & Verkoelen CF, eds), pp. 59–60. Shaker Publishing, Rotterdam.
6 Mensah P, Rodgers AL & Sturrock ED (2003) Inhibitory effect of urinary albumin from black and white South Africans on calcium oxalate monohydrate crystal aggregation. *Urol Res* **31**, 91.
7 Webber D, Rodgers AL & Sturrock ED (2002) Synergism between urinary prothrombin fragment 1 and urine: a comparison of inhibitory activities in stone-protein and stone-free population groups. *Clin Chem Laboratory Med* **40**, 930–936.
8 Knorle R, Schnierle P, Koch A, Buccholz NP, Hering F, Seiler H, Ackermann T & Rutishauer G (1994)

Tamm–Horsfall glycoprotein: role in inhibition and promotion of renal calcium oxalate stone formation studied with Fourier-transform infrared spectroscopy. *Clin Chem* **40**, 1739–1743.
9 Sumitra K, Pragasam V, Sakthivel R, Kalaiselvi P & Varalakshmi P (2005) Beneficial effect of vitamin E supplementation of the biochemical and kinetic properties of Tamm–Horsfall glycoprotein in hypertensive and hyperoxaluric patients. *Nephrol Dial Transplant* **20**, 1407–1415.
10 Atmani F, Lacour B, Jungers P, Drüeke T & Daudon M (1994) Reduced inhibitory activity of uronic-acid-rich protein in urine of stone formers. *Urol Res* **22**, 257–260.
11 Hallson PC, Choong SKS, Kasidas GP & Samuell CT (1997) Effects of Tamm–Horsfall protein with normal and reduced sialic acid content upon the crystallization of calcium phosphate and calcium oxalate in urine. *Br J Urol* **80**, 533–538.
12 Chen W-C, Lin H-S, Chen H-Y, Shih C-H & Li C-W (2001) Effects of Tamm–Horsfall protein and albumin on calcium oxalate crystallisation and importance of sialic acids. *Mol Urol* **5**, 1–5.
13 Konya E, Amasaki N, Umekawa T, Iguchi M & Kurita T (2002) Influence of urinary sialic acid on calcium oxalate crystal formation. *Urol Int* **68**, 281–285.
14 Nelsestuen GL & Suttie JW (1972) The carbohydrate of bovine prothrombin. Partial structural determination demonstrating the presence of α-galactose residues. *J Biol Chem* **247**, 6096–6102.
15 Magnusson S, Petersen TE, Sottrup-Jensen L & Claeys H (1975) Complete primary structure of prothrombin: isolation, structure and reactivity of ten carboxylated glutamic acid residues and regulation of prothrombin activation by thrombin. In *Proteases and Biological Control* (Reich E, Rifkin DB & Shaw E, eds), pp. 123–149. Cold Spring Harbor Laboratory, Cold Spring Harbor, New York.
16 Mizuochi T, Yamashita K, Fujikawa K, Kisiel W & Kobata A (1979) The carbohydrate of bovine prothrombin. *J Biol Chem* **254**, 6419–6425.
17 Harlos K, Boys CWG, Holland SK, Esnouf MP & Blake CCF (1987) Structure and order of the protein and carbohydrate domains of prothrombin fragment 1. *FEBS Lett* **224**, 97–103.
18 Guile GR, Rudd PM, Wing DR, Prime SB & Dwek RA (1996) A rapid higher-resolution high-performance liquid chromatographic method for separating glycan mixtures and analyzing oligosaccharide profiles. *Anal Biochem* **240**, 210–226.
19 Harvey DJ (2005) Fragmentation of negative ions from carbohydrates: Part 3, Fragmentation of hybrid and complex *N*-linked glycans. *J Am Soc Mass Spectrom* **16**, 647–659.
20 Endo T (1999) O-mannosyl glycans in mammals. *Biochim Biophys Acta* **1473**, 237–246.
21 Royle L, Mattu TS, Hart E, Langridge JI, Merry AH, Murphy N, Harvey DJ, Dwek RA & Rudd PM (2002) An analytical and structural database provides a strategy for sequencing *O*-glycans from microgram quantities of glycoproteins. *Anal Biochem* **304**, 70–90.
22 Hesse A, Classen A, Knoll M, Timmermann F & Vahlensieck W (1986) Dependence of urine composition on the age and sex of healthy subjects. *Clin Chim Acta* **160**, 79–86.
23 Ljungghall S & Danielson BG (1984) A prospective study of renal stone recurrence. *Br J Urol* **56**, 122–124.
24 Scurr DS & Robertson WG (1986) Modifiers of calcium oxalate crystallization found in urine. III. Studies on the role of Tamm–Horsfall mucoprotein and of ionic strength. *J Urol* **136**, 505–507.
25 Cao LC, Boevé ER, Kok DJ, de Bruijn WC, de Water R, Romijn JC, Verkoelen CF & Schröder FH (1996) Oxidative modification of Tamm–Horsfall protein by hydrogen peroxide and ascorbate-Fe(III). In *Urolithiasis '96. Proceedings of the VIII International Symposium on Urolithiasis* (Pak CYC, Resnick MI & Preminger GM, eds), pp. 337–338. Millet the Printer, Dallas, TX.
26 Grover PK & Ryall RL (1999) Inhibition of calcium oxalate crystal growth and aggregation by prothrombin and its fragments in vitro. *Eur J Biochem* **263**, 50–56.
27 Riese RJ, Riese JW, Kleinman JG, Wiessner JH, Mandel GS & Mandel NS (1988) Specificity in calcium oxalate adherence to papillary epithelial cells in culture. *Am J Physiol* **255**, F1025–F1032.
28 Lieske JC, Leonard R & Toback FG (1995) Adhesion of calcium oxalate monohydrate crystals to renal epithelial cells is inhibited by specific anions. *Am J Physiol* **268**, F604–F612.
29 Verkoelen CF, Romijn JC, de Bruijn WC, Boeve ER, Cao L & Schroder FH (1995) Association of calcium oxalate monohydrate crystals with MDCK cells. *Kidney Int* **48**, 129–138.
30 Lieske JC & Toback FG (1996) Interaction of urinary crystals with renal epithelial cells in the pathogenesis of nephrolithiasis. *Semin Nephrol* **6**, 458–473.
31 Lieske JC, Deganello S & Toback FG (1999) Cell–crystal interactions and kidney stone formation. *Nephron* **81**, 8–17.
32 Kumar V, de la Vega LP, Farell G & Lieske JC (2005) Urinary macromolecular inhibition of crystal adhesion to renal epithelial cells is impaired in male stone formers. *Kidney Int* **68**, 1784–1792.
33 Asselman M & Verkoelen CF (2002) Crystal–cell interaction in the pathogenesis of kidney stone disease. *Curr Opin Urol* **12**, 271–276.
34 Lieske JC, Toback FG & Deganello S (2001) Sialic-acid containing glycoproteins on renal cells determine the nucleation of calcium oxalate dihydrate crystals. *Kidney Int* **60**, 1784–1791.

35 Tiselius HG, Bek-Jensen H, Fornander AM & Nilsson MA (1995) Crystallization properties in urine from calcium oxalate stone formers. *J Urol* **154**, 940–946.
36 Borghi L, Guerra A, Meschi T, Briganti A, Schianchi T, Allegri F & Novarini A (1999) Relationship between supersaturation and calcium oxalate crystallization in normals and idiopathic calcium oxalate stone formers. *Kidney Int* **55**, 1041–1050.
37 Dean CJ, Macardle PJ & Ryall RL (2000) The effect of the presence of calcium oxalate crystals on the measurement of prothrombin fragment 1 in urine. In *Urolithiasis 2000* (Rodgers AL, Hibbert BE, Hess B, Khan SR & Preminger GM, eds), pp. 150–152. University of Cape Town, Cape Town.
38 Küster B, Wheeler F, Hunter AP, Dwek RA & Harvey DJ (1997) Sequencing of N-linked oligosaccharides directly from protein gels: in-gel deglycosylation followed by matrix-assisted laser desorption/ionisation mass spectrometry and normal-phase high-performance liquid chromatography. *Anal Biochem* **250**, 82–101.
39 Radcliffe CM, Diedrich G, Harvey DJ, Dwek RA, Cresswell P & Rudd PM (2002) Identification of specific glycoforms of major histocompatibility complex class I heavy chains suggests that class I peptide loading is an adaptation of the quality control pathway involving calreticulin and ERp57. *J Biol Chem* **277**, 46415–46423.
40 Patel T, Bruce J, Merry A, Bigge C, Wormald M, Jaques A & Parekh R (1993) Use of hydrazine to release in intact and unreduced form both *N*- and *O*-linked oligosaccharides from glycoproteins. *Biochemistry* **32**, 679–693.
41 Zamze S, Harvey DJ, Chen YJ, Guile GR, Dwek RA & Wing DR (1998) Sialylated N-glycans in adult rat brain tissue: a widespread distribution of disialylated antennae in complex and hybrid structures. *Eur J Biochem* **258**, 243–270.
42 Harvey DJ (1993) Quantitative aspects of the matrix-assisted laser desorption mass spectrometry of complex oligosaccharides. *Rapid Commun Mass Sp* **7**, 614–619.
43 Kraulis PJ (1991) *MOLSCRIPT*: a program to produce both detailed and schematic plots of protein structures. *J Appl Crystallogr* **24**, 946–950.